ACS Pharmacology & Translational Science

pubs.acs.org/ptsci

Article

Ebselen, Disulfiram, Carmofur, PX-12, Tideglusib, and Shikonin Are Nonspecific Promiscuous SARS-CoV-2 Main Protease Inhibitors

Chunlong Ma, Yanmei Hu, Julia Alma Townsend, Panagiotis I. Lagarias, Michael Thomas Marty, Antonios Kolocouris, and Jun Wang*

Cite This: *ACS Pharmacol. Transl. Sci.* 2020, 3, 1265−1277

Read Online

ACCESS | Metrics & More | Article Recommendations

ABSTRACT: Among the drug targets being investigated for SARS-CoV-2, the viral main protease (M^{pro}) is one of the most extensively studied. M^{pro} is a cysteine protease that hydrolyzes the viral polyprotein at more than 11 sites. It is highly conserved and has a unique substrate preference for glutamine in the P1 position. Therefore, M^{pro} inhibitors are expected to have broad-spectrum antiviral activity and a high selectivity index. Structurally diverse compounds have been reported as M^{pro} inhibitors. In this study, we investigated the mechanism of action of six previously reported M^{pro} inhibitors, ebselen, disulfiram, tideglusib, carmofur, shikonin, and PX-12, using a consortium of techniques including FRET-based enzymatic assay, thermal shift assay, native mass spectrometry, cellular antiviral assays, and molecular dynamics simulations. Collectively, the results showed that the inhibition of M^{pro} by these six compounds is nonspecific and that the inhibition is abolished or greatly reduced with the addition of reducing reagent 1,4-dithiothreitol (DTT). Without DTT, these six compounds inhibit not only M^{pro} but also a panel of viral cysteine proteases including SARS-CoV-2 papain-like protease and $2A^{pro}$ and $3C^{pro}$ from enterovirus A71 (EV-A71) and EV-D68. However, none of the compounds inhibits the viral replication of EV-A71 or EV-D68, suggesting that the enzymatic inhibition potency IC_{50} values obtained in the absence of DTT cannot be used to faithfully predict their cellular antiviral activity. Overall, we provide compelling evidence suggesting that these six compounds are nonspecific SARS-CoV-2 M^{pro} inhibitors and urge the scientific community to be stringent with hit validation.

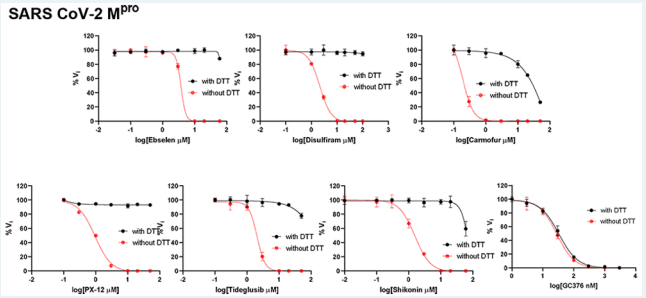

KEYWORDS: *SARS-CoV-2, main protease, 3CL protease, ebselen, carmofur, GC376*

A new coronavirus, SARS-CoV-2, started to circulate among humans in late 2019 and quickly evolved to be a global pandemic. As of August 31, 2020, there have been more than 6 million positive cases with over 183 000 deaths in the United States alone. The origin of SARS-CoV-2 is still under investigation, and the closest strain is the bat coronavirus RaTG13, which shares 96% sequence similarity with SARS-CoV-2.[1] It is unknown whether SARS-CoV-2 transmitted directly from bats to humans or through an intermediate host.[2] There are currently no vaccines or antiviral drugs available for SARS-CoV-2. Encouraging progress has been made in vaccine development, and several RNA-, DNA-, and adenovirus-based vaccine candidates are now in phase III clinical trials.[3] For small-molecule antivirals, remdesivir was granted emergency use authorization in the United States.

SARS-CoV-2 is an enveloped, positive-sense, single-stranded RNA virus that belongs to the betacoronavirus genera, which also includes SARS-CoV, MERS-CoV, HCoV-OC43, and HCoV-HKU1. SARS-CoV-2 shares ∼80% sequence similarity with SARS-CoV. As such, many of the reported antivirals against SARS-CoV-2 were originally developed for either SARS-CoV or other related coronaviruses.[4] SARS-CoV-2 infects ACE2-expressing cells and enters the cell through either direct cell surface fusion or the endosomal pathway.[5] For direct cell surface fusion, the host membrane protease TMPRSS2 cleaves the viral spike protein, triggering viral membrane fusion with the host cell membrane.[6] For endosomal entry, cathepsin L mediates the cleavage of viral spike protein.[7] Once the viral RNA is released in the cytoplasm, it undergoes translation into viral polyproteins pp1a and pp1ab, which are subsequently cleaved by two viral proteases, the main protease (M^{pro}), also called 3-chymotrypsin-like protease ($3CL^{pro}$), and the papain-like protease (PL^{pro}). The released viral proteins can then assemble to form the viral polymerase RdRp complex to catalyze the replication

Received: September 8, 2020
Published: October 9, 2020

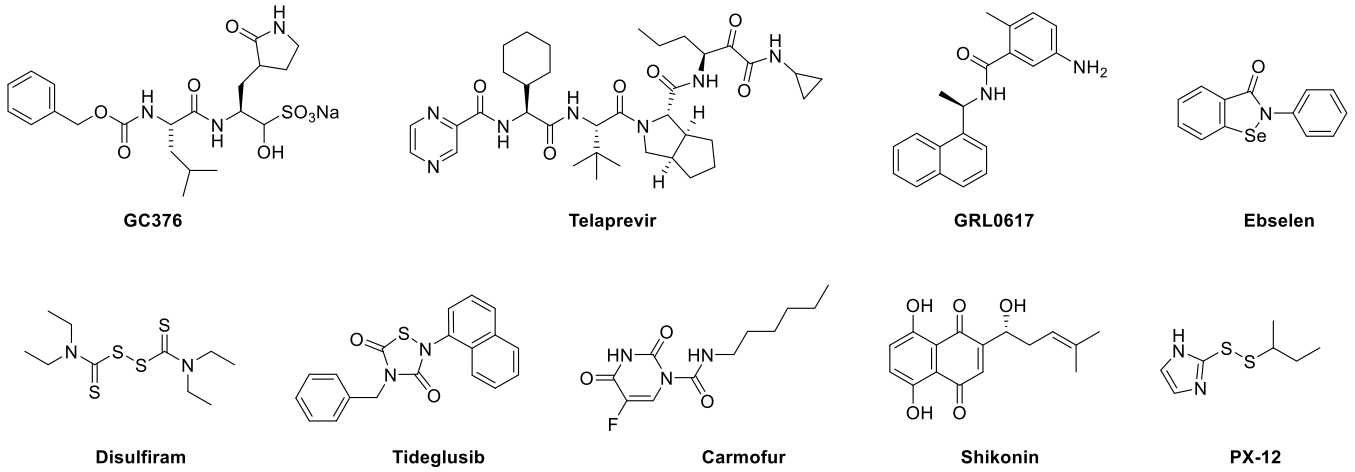

Figure 1. Chemical structures of protease inhibitors investigated in this study.

of viral RNA. Finally, progeny virions are released from the infected cells through exocytosis and are ready for the next round of infection.

Compounds that interfere with any step in the viral life cycle can theoretically inhibit viral replication. Among the list of drug targets pursued as SARS-CoV-2 small-molecule antivirals, the viral polymerase RdRp and the protease M^{pro} are the most extensively studied. The RdRp inhibitor remdesivir received emergency use authorization in the United States. It showed broad-spectrum antiviral activity against multiple coronaviruses in cell culture, including SARS-CoV-2, SARS-CoV, and MERS-CoV, and it also had *in vivo* efficacy in a SARS-CoV infection mouse model.[8] EIDD-2801, an RdRp inhibitor, is another promising drug candidate with broad-spectrum antiviral activity.[9] M^{pro} is a cysteine protease that cleaves the viral polyprotein at more than 11 sites. It has a unique substrate preference of glutamine at the P1 position, while no host protease is known to have such a preference.[10] As such, the most potent M^{pro} inhibitors such as GC376 and N3 all contain a 2-pyrrolidone substitution in the P1 position as a mimetic of the glutamine in the substrate. Several crystal structures of M^{pro} in complex with inhibitors have been solved, showing that the pyrrolidone forms multiple hydrogen bonds with the His163 and Glu166 side chains and the main chain of Phe140.[11−15] In addition to the classic pyrrolidone-containing M^{pro} inhibitors, several noncanonical M^{pro} inhibitors have also been reported with both enzymatic inhibition and cellular antiviral activity.[11,12] In this study, we aim to validate six previously reported M^{pro} inhibitors: ebselen, disulfiram, tideglusib, carmofur, shikonin, and PX-12 (Figure 1).[12] Among these six compounds, ebselen is a clinical candidate with anti-inflammatory and antioxidant activities. In preclinical studies, ebselen was reported to react with cysteine residues from completely unrelated proteins including the C-terminal domain of the HIV-1 capsid,[16] *Mycobacterium tuberculosis* transpeptidase LdtMt2,[17] glutamate dehydrogenase,[18] *Clostridium difficile* toxins TcdA and TcdB,[19] *Mycobacterium tuberculosis* (Mtb) antigen 85C enzyme,[20] hepatitis C virus NS3 helicase,[21] plant cysteine protease papain,[22] glutathione S-transferases,[22] and many others. However, the inhibition of papain by ebselen was abolished by the addition of reducing regents including glutathione (GSH), 2-mercaptoethanol, and sodium borohydride.[22] Ebselen was also reported to induce protein unfolding for the insulin-degrading enzyme.[23] Ebselen analogues were synthesized and were found to inhibit both SARS-CoV-2 M^{pro} and PL^{pro}.[24] Disulfiram inhibits a panel of diverse enzymes including methyltransferase,[25] urease,[26] and kinase[27] through reaction with the cysteine residues. A study also showed that disulfiram inhibits PL^{pro} from SARS-CoV and MERS-CoV with IC_{50} values of 14.2 and 22.7 μM, respectively.[28] However, the inhibition was completely lost in the presence of 5 mM β-mercaptoethanol (IC_{50} > 300 μM).[28] Carmofur inhibits human acid ceramidase by covalently modifying the catalytic C143 residue.[29] PX-12 inhibits tubulin polymerization through cysteine oxidation.[30] Tideglusib is an irreversible inhibitor of glycogen synthase kinase-3β (GSK-3β).[31]

Ebselen, disulfiram, carmofur, PX-12, tideglusib, and shikonin were recently reported as SARS-CoV-2 M^{pro} inhibitors with IC_{50} values ranging from 0.67 to 21.39 μM in the FRET-based enzymatic assay.[12] Among the six compounds, ebselen inhibited SARS-CoV-2 replication with an EC_{50} value of 4.67 ± 0.80 μM in plaque reduction assay. Disulfiram was able to reduce the viral replication by ∼30% in the viral titer reduction assay at 10 μM, while tideglusib, carmofur, and PX-12 had no significant antiviral effect. Intriguingly, in a follow up study, carmofur was shown to inhibit SARS-CoV-2 viral replication with an EC_{50} of 24.30 μM, and the X-ray crystal structure of M^{pro} with carmofur was solved (PDB: 7BUY).[32] The description of the enzymatic assay did not specify whether the reducing reagent dithiothreitol (DTT) was added or not. It is standard practice to add DTT or another reducing reagent such as glutathione (GSH) or β-mercaptoethanol (β-ME) in the enzymatic assay of cysteine protease to ensure that the enzyme is in the active form by reducing the catalytic cysteine residue as well as preventing nonspecific thiol reactive compounds from covalently modifying the catalytic cysteine.

The questions we are trying to address in this study are whether the inhibition of M^{pro} by these compounds is specific and whether their enzymatic inhibition potency IC_{50} values can be used to faithfully predict the cellular antiviral activity. In other words, do the reported IC_{50} values of ebselen, disulfiram, tideglusib, carmofur, shikonin, and PX-12 against SARS-CoV-2 M^{pro} reflect specific enzymatic inhibition, or are they due to nonspecific inactivation of the enzyme? We tested these compounds against a panel of related and unrelated viral cysteine proteases, the SARS-CoV-2 PL^{pro}, and the 2A protease ($2A^{pro}$) and 3C protease ($3C^{pro}$) from EV-A71 and EV-D68, in

https://dx.doi.org/10.1021/acsptsci.0c00130
ACS Pharmacol. Transl. Sci. 2020, 3, 1265−1277

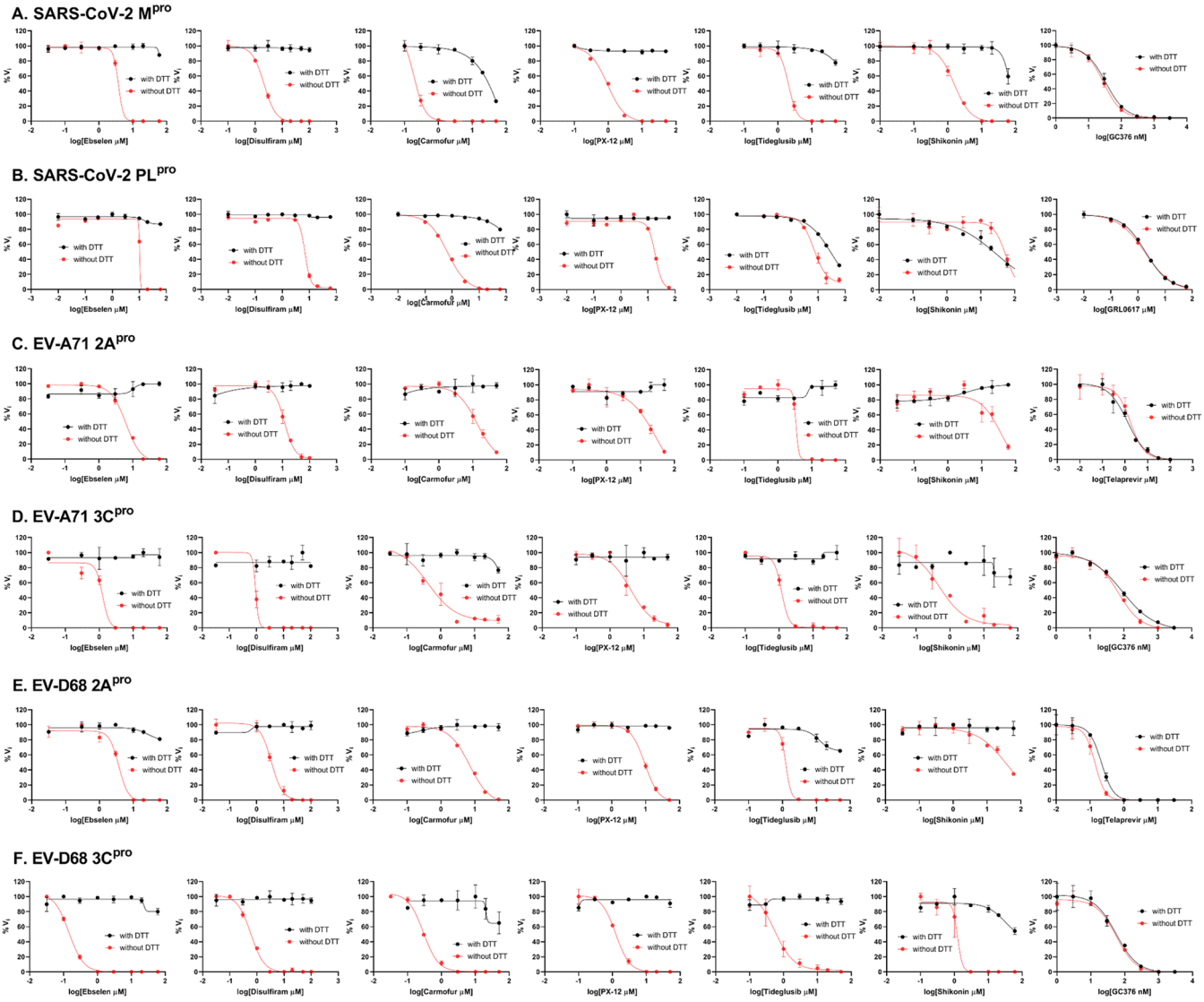

Figure 2. Enzymatic assay of SARS-CoV-2 M^{pro}, PL^{pro}, EV-A71 and EV-D68 $2A^{pro}$, and $3C^{pro}$ against inhibitors investigated in this study. (A) SARS-CoV-2 M^{pro}; (B) SARS-CoV-2 PL^{Pro}; (C) EV-A71 $2A^{pro}$; (D) EV-A71 $3C^{pro}$; (E) EV-D68 $2A^{pro}$; and (F) EV-D68 $3C^{pro}$. Protease was preincubated in their corresponding reaction buffer as described in the "Materials and Method" section with various concentrations of protease inhibitors in the presence of 4 mM DTT or in the absence of DTT at 30 °C for 30 min. The enzymatic reaction was initiated by adding the corresponding FRET substrate. The efficacy of these protease inhibitors in the presence of 4 mM DTT or in the absence of DTT was evaluated with a four-parameter dose−response curve function in prism 8 as described in the "Materials and Method" section.

a consortium of assays with or without DTT. Collectively, our results showed that in the absence of DTT, ebselen, disulfiram, tideglusib, carmofur, shikonin, and PX-12 nonspecifically inhibit all six viral cysteine proteases including SARS-CoV-2 M^{pro}. However, despite their potent inhibition of enzymatic activity of $2A^{pro}$ and $3C^{pro}$ from EV-A71 and EV-D68 in the FRET assay in the absence of DTT, none of the compounds showed cellular antiviral activity against EV-A71 and EV-D68. Therefore, it can be concluded that the enzymatic inhibition potency of cysteine protease inhibitors measured in the absence of DTT cannot be used to predict the cellular antiviral activity. Overall, although there is an immediate need for SARS-CoV-2 antivirals, the scientific community needs to be cautious about the nonspecific effect of promiscuous compounds, and secondary assays should be performed at the early stage to triage hits that lack translational potential.

RESULTS

Inhibition of SARS-CoV-2 M^{pro}, PL^{pro}, EV-A71 and EV-D68 $2A^{pro}$, and $3C^{pro}$ by Ebselen, Disulfiram, Carmofur, PX-12, Tideglusib, and Shikonin Is DTT-Dependent. To dissect the effect of DTT on the enzymatic inhibition of SARS-CoV-2 M^{pro} by ebselen, disulfiram, carmofur, PX-12, tideglusib, and shikonin, we performed dose−response titration in the FRET-based enzymatic assay with and without 4 mM DTT. A known M^{pro} inhibitor, GC376, was included as a positive control. It was found that all compounds inhibited M^{pro} in the absence of DTT (Figure 2A, red curves), and the IC_{50} values are generally in agreement with previous published results,[12] except for those of shikonin and PX-12, which showed more than 10-fold difference. However, none of the compounds showed potent inhibition against M^{pro} in the presence of 4 mM DTT (IC_{50} > 25 μM) (Figure 2A, black curves). Carmofur showed weak inhibition with an IC_{50} value of 28.2 ± 9.5 μM in

https://dx.doi.org/10.1021/acsptsci.0c00130
ACS Pharmacol. Transl. Sci. 2020, 3, 1265−1277

Table 1. Enzymatic Assay Results of Protease Inhibitors Investigated in This Study against SARS-CoV-2, EV-A71, and EV-D68 Proteases

	SARS-CoV-2 $M^{pro}IC_{50}$ (μM)	SARS-CoV-2 $PL^{pro}IC_{50}$ (μM) no DTT/with DTT	EV-A71 $2A^{pro}IC_{50}$ (μM) no DTT/with DTT	EV-A71 $3C^{pro}IC_{50}$ (μM) no DTT/with DTT	EV-D68 $2A^{pro}IC_{50}$ (μM) no DTT/with DTT	EV-D68 $3C^{pro}IC_{50}$ (μM) no DTT/with DTT
GC376	0.03 ± 0.01/0.03 ± 0.01	N.T.	N.T.	0.06 ± 0.02/ 0.08 ± 0.02	N.T.	0.06 ± 0.01/ 0.05 ± 0.02
telaprevir	N.T.	N.T.	1.8 ± 0.9/1.3 ± 0.6	N.T.	0.1 ± 0.0/0.2 ± 0.0	N.T.
GRL0617	N.T.	1.8 ± 0.2/1.9 ± 0.2	N.T.	N.T.	N.T.	N.T.
ebselen	3.7 ± 2.4/>60 **0.67 ± 0.09**(reported)[a]	10.3 ± 8.9/>60	5.9 ± 1.1/>60	1.2 ± 0.7/>60	3.6 ± 1.0/>60	0.1 ± 0.0/>60
disulfiram	2.1 ± 0.3/>60 **9.35 ± 0.18** (reported)	6.9 ± 4.2/>60	11.8 ± 2.1/>60	1.0 ± 0.6/>60	3.5 ± 0.5/>60	0.6 ± 0.1/>60
tideglusib	2.1 ± 0.3/>60 **1.55 ± 0.30** (reported)	7.1 ± 1.4/30.4 ± 17.1	3.4 ± 2.9/>60	1.2 ± 0.1/>60	1.3 ± 0.7/>60	0.6 ± 0.3/>60
carmofur	0.2 ± 0.1/28.2 ± 9.5 **1.82 ± 0.06** (reported)	0.7 ± 0.1/>60	12.9 ± 4.5/>60	0.4 ± 0.2/>60	6.4 ± 1.3/>60	0.3 ± 0.0/>60
shikonin	1.5 ± 0.3/>60 **15.75 ± 8.22** (reported)	55.3 ± 17.7/28.2 ± 12.5	36.0 ± 20.5/>60	0.5 ± 0.2/>60	37.0 ± 14.2/>60	1.2 ± 0.7/>60
PX-12	0.9 ± 0.2/>60 **21.39 ± 7.06** (reported)	18.7 ± 2.6/>60	16.9 ± 9.2/>60	4.1 ± 1.9/>60	9.3 ± 4.2/> 60	1.2 ± 0.2/> 60

[a]The values shown in bold were reported in reference[12] N.T. = not tested.

the presence of DTT (Table 1). In contrast, GC376 showed consistent inhibition against M^{pro} both in the absence and presence of DTT with IC_{50} values of 0.03 μM and 0.03 μM, respectively (Figure 2A, last column; Table 1). These results suggest that the claimed inhibition of M^{pro} by these six compounds might not be target-specific. To test this hypothesis, we next tested these six compounds against five other viral cysteine proteases, among which SARS-CoV-2 PL^{pro}, EV-A71 $2A^{pro}$, and EV-D68 $2A^{pro}$ have no sequence similarity with M^{pro}, while EV-A71 $3C^{pro}$ and EV-D68 $3C^{pro}$ share similar chymotrypsin-like folding with M^{pro}, despite only showing 16.3 and 19.6% sequence similarities with M^{pro}. GRL0617 was included as a positive control for SARS-CoV-2 PL^{pro},[33] and telaprevir was included as a positive control for EV-A71 $2A^{pro}$ and EV-D68 $2A^{pro}$.[34] GC376 was used as a positive control for both EV-A71 $3C^{pro}$ and EV-D68 $3C^{pro}$. If the inhibition of M^{pro} by ebselen, disulfiram, carmofur, PX-12, tideglusib, and shikonin is specific, in either the absence or the presence of DTT, then these six compounds are expected to show little or no inhibition against the unrelated SARS-CoV-2 PL^{pro}, EV-A71 $2A^{pro}$, and EV-D68 $2A^{pro}$. For SARS-CoV-2 PL^{pro}, we observed results similar to those for SARS-CoV-2 M^{pro}: All compounds displayed a potent inhibitory effect in the absence of DTT, while little or no inhibition was observed in the presence of DTT (Figure 2B). Shikonin was less potent against PL^{pro} than against M^{pro} in the absence of DTT with IC_{50} values of 1.5 and 55.3 μM, respectively (Table 1). The potency of shikonin increased about 2-fold, and the IC_{50} values were 55.3 and 28.2 μM with and without DTT, respectively (Table 1). As expected, the noncovalent SARS-CoV-2 PL^{pro} inhibitor GRL0617[35] inhibits SARS-CoV-2 PL^{pro} similarly in the present or the absence of 4 mM DTT (Figure 2B, last column). For EV-A71 and EV-D68 $2A^{pro}$ and $3C^{pro}$, we observed trends similar to that of M^{pro}: All six compounds showed potent enzymatic inhibition in the absence of DTT, and the inhibition was abolished with the addition of DTT (Figures 2C–F). In contrast, there is no significant shift of the potency with and without DTT for GC376 in inhibiting EV-A71 $3C^{pro}$ (Figure 2D) and EV-D68 $3C^{pro}$ (Figure 2F) and for telaprevir in inhibiting EV-A71 $2A^{pro}$ (Figure 2C) and EV-D68 $2A^{pro}$ (Figure 2E).

Next, we tested whether another reducing agent, GSH, could also abolish the inhibitory effect of these promiscuous inhibitors against SARS-CoV-2 M^{pro}. Ebselen and disulfiram were chosen as representative examples. In the absence of 4 mM DTT or 1 mM GSH, ebselen and disulfiram completely inhibit M^{pro} enzymatic activity at 20 μM (Figure 3); however,

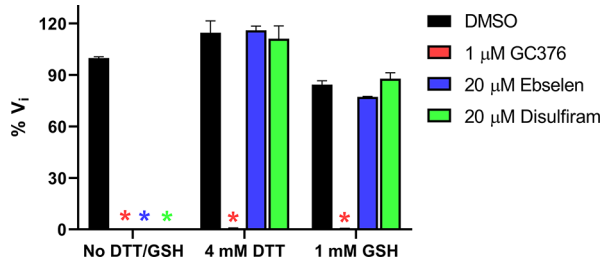

Figure 3. Effect of glutathione (GSH) on the inhibition of ebselen and disulfiram against SARS-CoV-2 M^{pro}. SARS-CoV-2 M^{pro} protein (100 nM) was preincubated in SARS-CoV-2 M^{pro} reaction buffer with the testing protease inhibitors in the absence of DTT or GSH, or in the presence of 4 mM DTT or 1 mM GSH at 30 °C for 30 min. The enzymatic reaction was initiated by adding 10 μM SARS-CoV-2 M^{pro} FRET substrate. The initial enzymatic reaction velocity was measured and normalized to the condition that no protease inhibitor (DMSO) and no DTT/GSH was present in the reaction buffer.

no inhibition was observed for ebselen and disulfiram when either 4 mM DTT or 1 mM GSH was present in the reaction buffer (Figure 3). In contrast, the inhibition by the positive control GC376 was not affected by the reducing agent DTT or GSH.

Collectively, the enzymatic assay results suggest that ebselen, disulfiram, carmofur, PX-12, tideglusib, and shikonin are promiscuous cysteine protease inhibitors that inhibit not only M^{pro} but also five other related and unrelated viral cysteine proteases including SARS-CoV-2 PL^{pro} and EV-A71 and EV-D68 $2A^{pro}$ and $3C^{pro}$ in the absence of DTT, and the

https://dx.doi.org/10.1021/acsptsci.0c00130
ACS Pharmacol. Transl. Sci. 2020, 3, 1265–1277

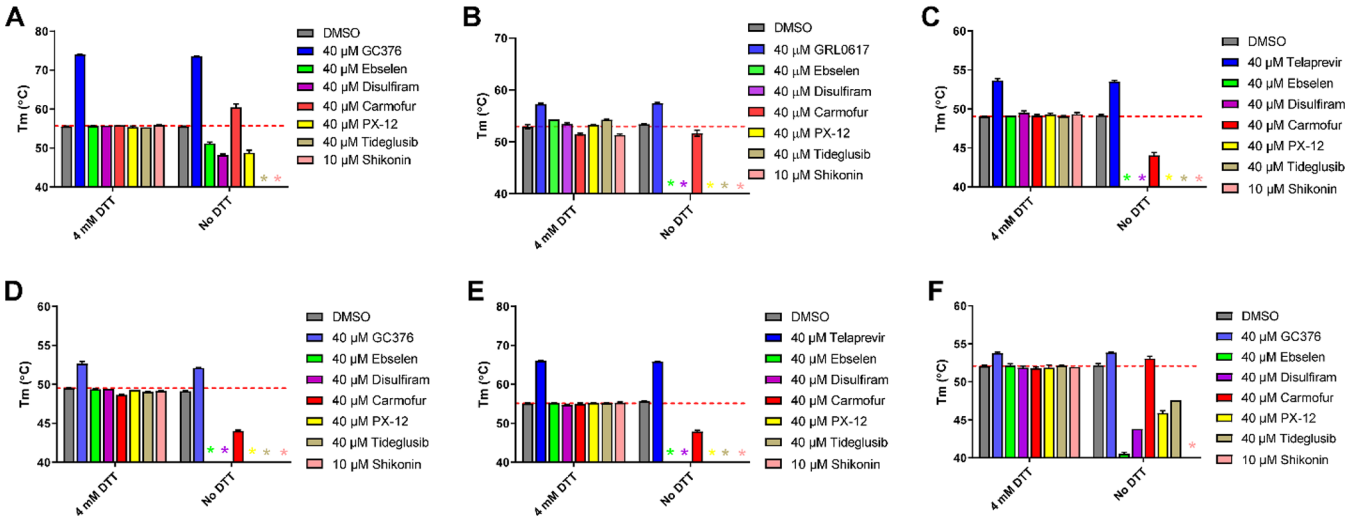

Figure 4. Thermal shift binding assay of SARS-CoV-2, EV-A71, and EV-D68 proteases against inhibitors investigated in this study. (A) SARS-CoV-2 M^{pro}, (B) SARS-CoV-2 PL^{Pro}, (C) EV-A71 $2A^{pro}$, (D) EV-A71 $3C^{pro}$, (E) EV-D68 $2A^{pro}$, and (F) EV-D68 $3C^{pro}$. Protease (3 μM) in its corresponding enzymatic reaction buffer in the presence of 4 mM DTT or in the absence of DTT was preincubated with DMSO or 40 μM protease inhibitors at 30 °C for 30 min (shikonin was tested at 10 μM because 40 μM shikonin completely quenches SYPRO orange dye fluorescence signal). The melting temperature (T_m) was calculated as the mid log of the transition phase from the native to the denatured protein using a Boltzmann model.[36] * indicates that a fluorescence peak was not observed in the melting curve; the red dashed line shows the protease T_m with DMSO in the presence of 4 mM DTT.

inhibition is abolished with the addition of a reducing reagent, either DTT or GSH.

Ebselen, Disulfiram, Carmofur, PX-12, Tideglusib, and Shikonin Did Not Bind to SARS-CoV-2 M^{pro} in the Presence of DTT in the Thermal Shift Assay. To investigate whether ebselen, disulfiram, carmofur, PX-12, tideglusib, and shikonin bind directly to M^{pro} or other related and unrelated cysteine proteases, we performed a thermal shift binding assay. In the thermal shift binding assay, a temperature gradient is applied to denature a protein in the presence of a fluorescence dye. When the protein unfolds, the hydrophobic region is exposed to the fluorescence dye, and an increased fluoresce signal is observed. Specific binding of a small molecule to the native state of a protein usually stabilizes the protein, leading to a shift of the melting temperature (ΔT_m).[34,36−38] Here we measured the T_m change upon addition of these six compounds in the presence or absence of 4 mM DTT against six viral cysteine proteases including M^{pro}. All compounds were tested at 40 μM except shikonin, which was tested at 10 μM as it quenches the SYPRO orange dye fluorescence signal at 40 μM. Compounds were preincubated with 3 μM protease in its corresponding enzymatic reaction buffer at 30 °C for 30 min with or without 4 mM DTT, then a 20−90 °C temperature gradient was applied and T_m was calculated. As expected, for the positive controls in the presence of 4 mM DTT, a significant T_m increase was observed in the binding of GC376 to SARS-CoV-2 M^{pro} (Figure 4A), EV-A71 $3C^{pro}$ (Figure 4D), and EV-D68−$3C^{pro}$ (Figure 4F). Binding of GRL0617 to SARS-CoV-2 PL^{pro} also led to significant stabilization (Figure 4B). Similarly, binding of telaprevir to EV-A71 $2A^{pro}$ and EV-D68 $2A^{pro}$ increased the T_m (Figure 4C,E). Importantly, positive control compounds showed consistent T_m shifts with and without DTT (Figure 4A−F). In contrast, in the presence of 4 mM DTT, no T_m change was observed with the addition of ebselen, disulfiram, carmofur, PX-12, tideglusib, and shikonin to all six proteases, suggesting that none of the compounds binds to any of these proteases (Figures 4A−F). In the absence of DTT, upon the addition of these six compounds, a decrease of T_m or no change was observed (Figures 4A−F), except in the cases when carmofur binds to SARS-CoV-2 M^{pro} and EV-D68 $3C^{pro}$, in which T_m increases of 4.76 and 0.87 °C were observed, respectively (Figure 4A,F). A negative T_m shift means binding of a small molecule to a protein leads to the destabilization.

Taken together, when 4 mM DTT was present in the assay buffer, there was no binding between the six viral cysteine proteases and the six compounds ebselen, disulfiram, carmofur, PX-12, tideglusib, and shikonin; without DTT, these compounds appear to nonspecifically bind to these proteases, leading to destabilization.

Ebselen, Disulfiram, PX-12, Tideglusib, and Shikonin Did Not Bind to SARS-CoV-2 M^{pro}, while Carmofur Showed Binding in the Presence of DTT in the Native Mass Spectrometry Binding Assay. To corroborate the results from the thermal shift binding assay, we next performed native mass spectrometry (MS)-based binding assays. Native MS analysis revealed that SARS-CoV-2 M^{pro} forms a dimer that was measured to have a mass of 67 595 Da (Figure 5A). A small abundance of monomer was measured with a mass of 33 796 Da, but the intact dimer was the predominant signal (data not shown). The addition of GC376 revealed that up to two ligands bound per dimer (Figure 5B), suggesting a binding ratio of one drug per monomer, which is consistent with its mechanism of action revealed by X-ray crystallography.[11] The addition of 4 mM DTT shifted the equilibrium to one ligand per dimer (Figure 5C). When carmofur was added to SARS-CoV-2 M^{pro}, it bound up to three ligands per dimer, with the most abundant signal being that for the two bound per dimer (Figure 5J). When 4 mM DTT was added, it disrupted the ligand binding of carmofur, with the most abundant signal being that for the dimer without ligand bound (Figure 5K). Nevertheless, signals corresponding to one ligand per dimer and two ligands per dimer could still be detected, suggesting that carmofur has moderate binding toward SARS-CoV-2 M^{pro}

https://dx.doi.org/10.1021/acsptsci.0c00130
ACS Pharmacol. Transl. Sci. 2020, 3, 1265−1277

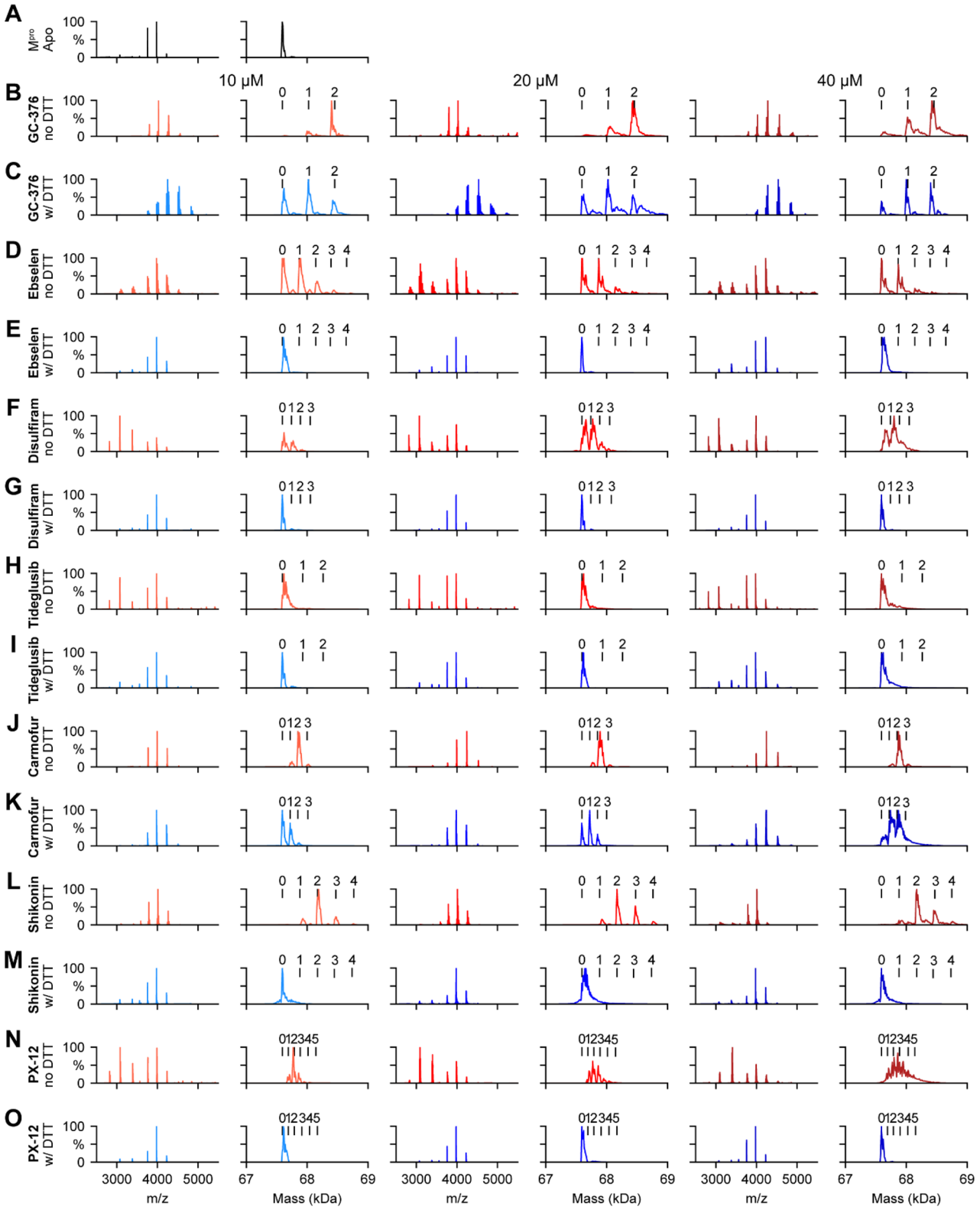

Figure 5. Native MS binding assay of SARS-CoV-2 M^{pro} to different protease inhibitors investigated in this study. The native mass spectra (columns 1, 3, and 5) and deconvolved mass distributions (columns 2, 4, and 6) of SARS-CoV-2 M^{pro} without added compound (A) and with added GC376 (B and C), ebselen (D and E), disulfiram (F and G), tideglusib (H and I), carmofur (J and K), shikonin (L and M), and PX-12 (N and O). Spectra are shown without DTT (B, D, F, H, J, L, and N) and with 4 mM DTT (C, E, G, I, K, M, and O) and for the drug concentration of 10 μM (columns 1 and 2), 20 μM (columns 3 and 4), and 40 μM (columns 5 and 6). Dimer, one-drug-bound dimer, two-drug-bound dimer, three-drug-bound dimer, four-drug-bound dimer, and five-drug-bound dimer were labeled as 0, 1, 2, 3, 4, and 5, respectively.

even in the presence of DTT (Figure 5K). This result is consistent with our enzymatic assay result, which showed that carmofur inhibits M^{pro} with an IC_{50} of 28.2 ± 9.5 μM in the presence of 4 mM DTT (Figure 2A). Taken together, the

https://dx.doi.org/10.1021/acsptsci.0c00130
ACS Pharmacol. Transl. Sci. 2020, 3, 1265−1277

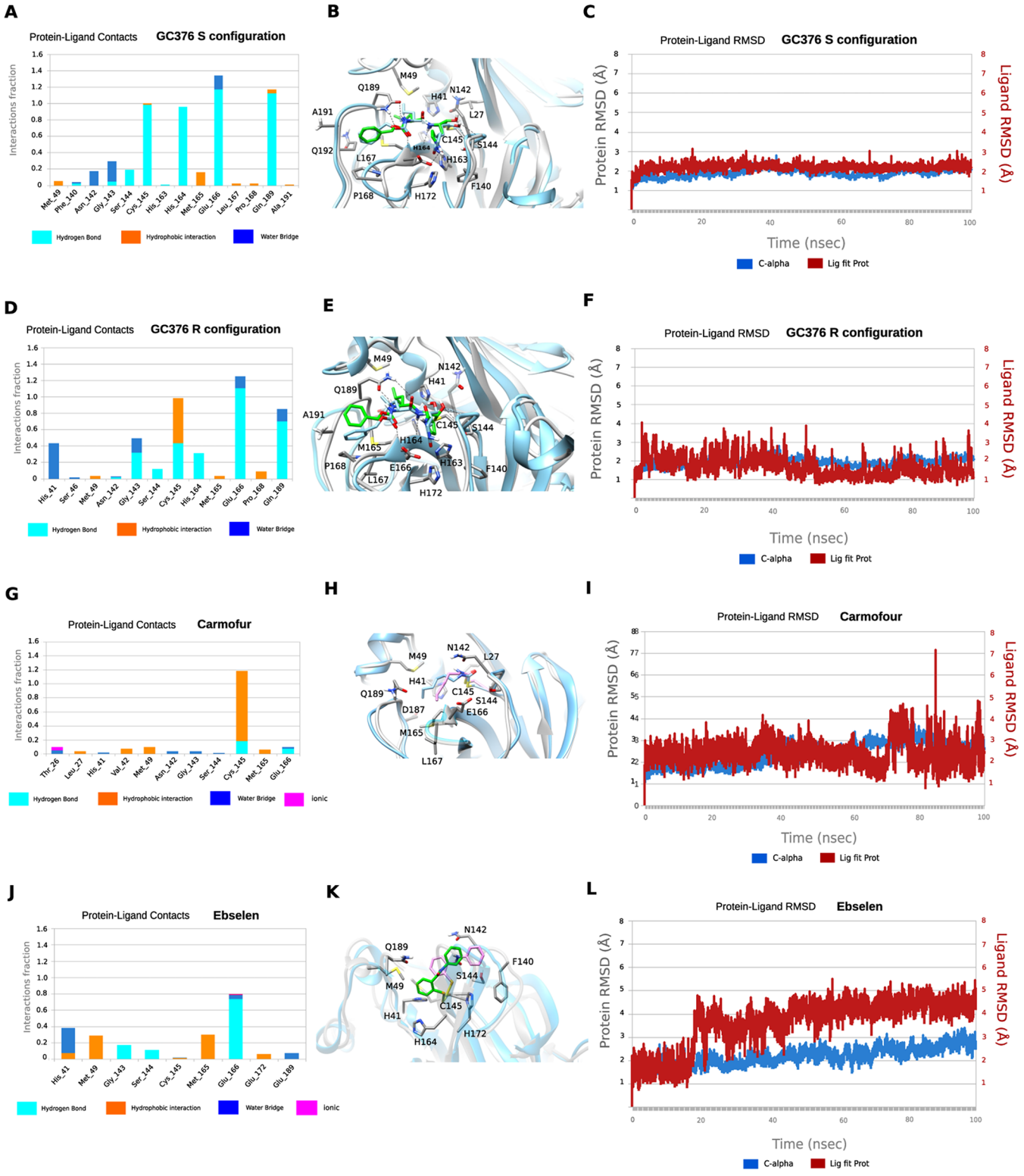

Figure 6. MD simulations of SARS-CoV-2 M^{pro} with its inhibitors. (A, D, G, and J) Color key: hydrogen bonding interactions bar, light blue; van der Waals, orange; water bridges, blue; and ionic interactions, magenta. Interactions are plotted from 100 ns MD simulations for the complexes between the covalently bound GC376-*S*, GC376-*R*, carmofur and ebselen inside SARS-CoV-2 M^{pro}. They are considered important when frequency bar is ≥0.2. (B, E, H, and K) The last snapshots of the above-mentioned 100 ns-MD simulated complexes were overlaid with experimental structures with PDB IDs 6WTT for GC376-*S* and GC376-*R* and 7BUY for carmofur and a covalent docking pose for ebselen. (C, F, I, and L) RMSD plots of C*α* carbons (blue diagram, left axis) and of ligand (red diagram, right axis) of the above-mentioned 100 ns-MD simulated complexes. The starting structures are the experimental determined structures with PDB IDs of 6WTT GC376-*S* and GC376-*R* and 7BUY for carmofur and a covalent docking pose for ebselen.

https://dx.doi.org/10.1021/acsptsci.0c00130
ACS Pharmacol. Transl. Sci. 2020, 3, 1265−1277

inhibition of M^{pro} by carmofur has certain degree of specificity, although the potency is moderate. Similarly, disulfiram, ebselen, and PX-12 bound up to three, four, and five ligands per dimer respectively (Figure 5F,D,N) in the absence of DTT, and the addition of 4 mM DTT completely disrupted this ligand binding (Figure 5G,E,O), and only the dimer signal without ligand was detected. The complete disruption of this ligand binding with the addition of DTT suggests that these compounds bind nonspecifically to SARS-CoV-2 M^{pro}. Shikonin was found to bind up to four ligands per dimer to SARS-CoV-2 M^{pro} (Figure 5L), and this binding was completely disrupted upon addition of 4 mM DTT (Figure 5M). Tideglusib did not bind to M^{pro} in either the absence or the presence of 4 mM DTT at concentrations ranging from 10 to 40 μM (Figure 5H,I).

The observation that ebselen, disulfiram, carmofur, shikonin, and PX-12 can bind to M^{pro} with more than two ligands per dimer in the absence of DTT indicates that these compounds might not only modify the catalytic cysteine C145 but also possibly bind to allosteric sites or covalently modify other cysteine residues on M^{pro}.

Molecular Dynamics (MD) Simulations of the Binding of M^{pro} to GC376, Carmofur, and Ebselen. We performed MD simulations to compare the stability of the binding interactions identified in the X-ray structures of SARS-CoV-2 M^{pro} in complex with GC376 and carmofur. The MD simulations of M^{pro} with ebselen were carried using the highest scored docking pose.

Our previous study showed that when GC376 binds to the SARS-CoV-2 M^{pro}, the covalent thioketal adduct can adapt both the *S*- and *R*-configuration.[11] The MD simulations showed that the complexes formed with GC376 in either the *S*- or *R*-configuration did not deviate from the starting X-ray structures with an RMSD in protein and ligand positions from the X-ray structure smaller than ca. 2 Å for the protein and smaller than ca. 2.3 Å for the ligand (Figure 6C,F). The MD simulations verified stabilizing interactions observed in the X-ray structure, which remain stable inside the binding cavity as shown in the frequency interaction plot in Figure 6A,D. From the protein−ligand contact plots of the GC376 in the *S*-configuration (Figure 6A,B), it is shown that it forms multiple hydrogen bonds, i.e., (a) between the thiohemiketal P1 hydroxyl group and C145 peptidic NH; (b) between 2-pyrrolidone's NH at the P1 and the side chain of E166 and between peptidic NH at P1 with H164 side chain imidazole; (c) between carbamate CO, NH, and benzyloxy oxygen at P2 with peptidic NH at M165, Q189 side chain CO, and Q189 side chain NH, respectively. In the X-ray structure, the pyrrolidone's CO forms a hydrogen bond with H163 side chain imidazole; the MD simulation plot in Figure 6A represents an average description of the interactions from an ensemble and not from a single snapshot in the X-ray structure. The polar 2-pyrrolidone group is oriented toward the solvent-exposed S1 pocket, while isobutyl group at P2 position is oriented comfortably toward the hydrophobic S2 site formed by H41, M49, and M169. The benzyloxy group facing toward L167 moves freely in the area between Q189, A191, Q192, L167, and P168 (Figure 6B). In the *R*-configuration, GC376 is stabilized through hydrogen bonding interaction with C145, H164, E166, and Q189, as well as G143 and H41, but the frequency of hydrogen bond interactions is less when pyrrolidone side chain is buried in the S1 pocket (Figure 6D,E).

In contrast to the numerous stabilizing interactions of GC376 in both the *S*- and *R*-configurations, carmofur interacts mainly with C145 through van der Waals and hydrogen bonding interactions (Figure 6G,H). In carmofur, the MD simulations show that the RMSD in protein and ligand positions from the X-ray structure are both ca. 3 Å for the protein and the ligand. The hexyl side chain is oriented inside the binding cavity, from S1 to S3, but the interactions of the drugs cannot be specific for M^{pro} without directing hydrogen bond and van der Waals interactions complementary to the cavity. Ebselen interacts through hydrogen bonding interactions mainly with E166 and van der Waals interactions with M49 and M165 in the hydrophobic S2 binding area. Similar to carmofur, these interactions are not adequate to effectively trap the small drug inside the wide binding area of M^{pro} (Figure 6J,K), and the drug can rotate around the phenyl−CO bond, resulting in a high RMSD of ca. 5.4 Å (Figure 6L). Compared to GC376, the protein−ligand contact plots of carmofur and ebselen suggest that these two compounds bind to SARS-CoV-2 M^{pro} with reduced affinity, corroborating with their nonspecific inhibition mechanism.

Ebselen, Disulfiram, Carmofur, PX-12, Tideglusib, and Shikonin Had No Cellular Antiviral Activity against EV-A71 and EV-D68. If the enzymatic inhibition potency IC_{50} values obtained in the absence of DTT can be used to faithfully predict the cellular antiviral activity, then one would expect all six compounds, ebselen, disulfiram, carmofur, PX-12, tideglusib, and shikonin, will have potent antiviral activity against EV-A71 and EV-D68. To test this hypothesis, the cellular antiviral activity of ebselen, disulfiram, carmofur, PX-12, tideglusib, and shikonin against EV-A71 and EV-D68 viruses were tested in RD cells using the viral cytopathic effect (CPE) assay.[34] GC376 and telaprevir were included as positive controls as $3C^{pro}$ and $2A^{pro}$ inhibitors. GC376 inhibited EV-A71 and EV-D68 with EC_{50} values of 0.2 and 0.9 μM, respectively (Table 2). Telaprevir inhibited EV-D68 with an EC_{50} of 0.4 μM (Table 2). However, none of the six compounds showed antiviral activity against either EV-A71 or EV-D68 at the highest nontoxic drug concentration (Table 2).

Table 2. Cellular Antiviral Assay Results of Ebselen, Disulfiram, Carmofur, PX-12, Tideglusib, and Shikonin against EV-A71 and EV-D68

	EV-A71 CPE assay $EC_{50}(\mu M)/CC_{50}$ (μM)[a]	EV-D68 CPE assay $EC_{50}(\mu M)/CC_{50}$ (μM)
GC-376	0.2 ± 0.1/>50	0.9 ± 0.0/>50
telaprevir	N.T.	0.4 ± 0.1/48.8 ± 4.1
ebselen	>20/17.0 ± 0.70	>10/5.4 ± 0.2
disulfiram	>10/8.3 ± 0.6	>3/1.5 ± 0.1
tideglusib	>20/16.6 ± 1.2	>20/12.8 ± 0.7
carmofur	>50/47.2 ± 4.8	>20/18.5 ± 1.5
shikonin	>1/0.8 ± 0.0	>1/0.4 ± 0.0
PX-12	>10/7.1 ± 0.5	>20/16.5 ± 2.4

[a]EC_{50} and CC_{50} (μM) = mean ± standard deviation. The values are the mean ± standard deviation from three replicates.

DISCUSSION

To combat the COVID-19 pandemic, researchers around the globe are racing to come up with effective countermeasures. Promising progress has been made in developing vaccines and antiviral drugs. Antivirals are necessary complements of

https://dx.doi.org/10.1021/acsptsci.0c00130
ACS Pharmacol. Transl. Sci. 2020, 3, 1265−1277

vaccines and are needed for postinfection treatment. Among the viral proteins under investigation as drug targets for SARS-CoV-2, the viral protein RdRp is the most extensively studied, which was followed by the viral protein M^{pro}.[39] Antiviral drug discovery targeting M^{pro} started with the initial efforts of developing of inhibitors against rhinovirus 3C protease ($3C^{pro}$). Rhinovirus $3C^{pro}$, enterovirus $3C^{pro}$, human norovirus 3CL protease, and coronavirus 3CL protease (M^{pro}) all share the same substrate preference for glutamate at the P1 position, suggesting that $3C^{pro}$ or $3CL^{pro}$ inhibitors are promising drug candidates for broad-spectrum antivirals. Over the past few decades, significant progress has been made in designing $3C^{pro}$ or $3CL^{pro}$ inhibitors. Rupintrivir (AG7088) and AG7404 are prominent examples of human rhinovirus $3C^{pro}$ inhibitors that have been evaluated in clinical trials for the treatment of rhinovirus infection. For coronaviruses, GC376 is one of the most advanced lead compounds. It showed broad-spectrum *in vitro* antiviral activity against SARS-CoV and MERS-CoV, and *in vivo* antiviral activity in cats infected with feline infectious peritonitis virus.[40,41] Given the sequence similarity between SARS-CoV-2 and SARS-CoV M^{pro}, it became apparent that existing $3C^{pro}$ or $3CL^{pro}$ inhibitors might be active against SARS-CoV-2 M^{pro}. Indeed, the most potent M^{pro} inhibitors reported so far such as N3, 13a, 13b, and GC376 all contain the pyrrolidone substitution in the P1 position, with variations in the reactive warhead and P2, P3, and P4 substitutions.[11−14] Interestingly, six compounds, ebselen, disulfiram, carmofur, PX-12, tideglusib, and shikonin, that share no structural similarity with GC376 were claimed as novel SARS-CoV-2 M^{pro} inhibitors.[12] MS/MS analysis revealed that ebselen, PX-12, and carmofur were able to covalently modify the catalytic cysteine C145 of SARS-CoV-2 M^{pro}.[12]

In line with these documented polypharmacology of ebselen, disulfiram, carmofur, PX-12, tideglusib, and shikonin, we are interested in validating these compounds against SARS-CoV-2 M^{pro} inhibition. Our enzymatic assay results showed that the inhibition of SARS-CoV-2 M^{pro} by these six compounds is dependent on the reducing reagent DTT. In the absence of DTT, all six compounds ebselen, disulfiram, carmofur, PX-12, tideglusib, and shikonin showed potent inhibition against not only M^{pro} but also two related viral proteases the EV-A71 and EV-D68 $3C^{pro}$, as well as three unrelated viral proteases, SARS-CoV-2 PL^{pro} and EV-A71 and EV-D68 $2A^{pro}$ (Figure 2). However, upon addition of 4 mM DTT, the broad-spectrum enzymatic inhibition of these compounds was largely diminished, except for carmofur and tideglusib, which had weak inhibition against M^{pro} and PL^{pro} with IC_{50} values of 28.2 and 30.4 μM, respectively (Figure 2; Table 1). In line with the enzymatic assay results, thermal shift binding assay and native MS assay showed that ebselen, disulfiram, PX-12, tideglusib, and shikonin did not bind to M^{pro} in the presence of DTT, while carmofur could still bind to M^{pro} with the addition of DTT (Figures 4 and 5). These results suggest that the inhibition of M^{pro} by carmofur has certain specificity, although the potency is relatively weak. In contrast, the inhibitory effect and binding of control compounds GC376 against M^{pro} and EV-A71 and EV-D68 $3C^{pro}$, GRL0618 against PL^{pro}, and telaprevir against EV-A71 and EV-D68 $2A^{pro}$ were not affected by the addition of DTT (Figures. 2, 4, and 5). MD simulations provided additional evidence showing that the drug-bound M^{pro} complex is more stable for specific inhibitor GC376 than for promiscuous compounds ebselen and carmofur (Figure 6). Furthermore, it is generally assumed that for specific inhibitors, the enzymatic inhibition potency IC_{50} value could be used to predict the cellular antiviral activity. However, despite their apparent inhibition of the EV-A71 and EV-D68 $2A^{pro}$ and $3C^{pro}$ in the absence of DTT (Table 1), none of the six compounds, ebselen, disulfiram, carmofur, PX-12, tideglusib, and shikonin, showed cellular antiviral activity against EV-A71 and EV-D68 in the CPE assay (Table 2). Therefore, caution should be taken when interpreting the enzymatic assay inhibition IC_{50} values of cysteine proteases obtained in the absence of reducing reagent such as DTT or GSH. In the absence of DTT, the apparent inhibition might be due to either alkylation or oxidation of the cysteine residue by reactive compounds. To rule out such a nonspecific effect, reducing reagents such as DTT, β-ME, or GSH should be added to the enzymatic buffer. Specific cysteine protease inhibitors should not show significant IC_{50} shift upon addition of reducing reagent in both the enzymatic assay and the binding assay. Moreover, counter-screening against unrelated cysteine proteases should also be performed as a secondary assay to confirm the specificity. Although these promiscuous compounds such as ebselen have been frequently highlighted as promising drug candidates,[42,43] the scientific community should be cautious in interpreting the pharmacology of these compounds and be aware of their nonspecific effects.

MATERIALS AND METHODS

Cell Lines and Viruses. Human rhabdomyosarcoma (RD) cells were maintained in Dulbecco's modified Eagle's medium (DMEM), supplemented with 10% fetal bovine serum (FBS) and 1% penicillin−streptomycin antibiotics. Cells were kept at 37 °C in a 5% CO_2 atmosphere. EV-D68 strain US/MO/14−18947 (ATCC NR-49129) was purchased from ATCC and amplified in RD cells prior to infection assays. EV-A71 strain 5865/SIN/000009 was obtained from Dr. Chan at the Department of Medical Microbiology, Faculty of Medicine, University of Malaya.[44]

Protein Expression and Purification. *SARS-CoV-2 M^{pro}.* SARS-CoV-2 M^{pro} gene from strain BetaCoV/Wuhan/WIV04/2019 in the pET29a(+) vector with *E. coli* codon optimization was ordered from GenScript (Piscataway, NJ). The expression and purification of SARS-CoV-2 M^{pro} was described as previously.[11]

SARS-CoV-2 PL^{pro}. SARS-CoV-2 papain-like protease (PL^{pro}) gene (ORF 1ab 1564−1876) from strain BetaCoV/Wuhan/WIV04/2019 with *E. coli* codon optimization was ordered from GenScript in the pET28b(+) vector. The pET28b(+) plasmid with SARS-CoV-2 PL^{pro} gene was transformed into BL21(DE3) cells with kanamycin selection. A single colony was picked to inoculate 10 mL of LB media and was cultured 37 °C overnight. This 10 mL culture was added to 1 L of LB media and grown to around OD_{600} of 0.8. This culture was cooled on ice for 15 min, then induced with 0.5 mM IPTG. Induced cultures were incubated at 18 °C for an additional 24 h and then harvested and lysed the same way as SARS-CoV-2 M^{pro} protein.[11] The supernatant was incubated with Ni-NTA resin for overnight at 4 °C on a rotator. The Ni-NTA resin was thoroughly washed with 30 mM imidazole in wash buffer (50 mM Tris [pH 7.5], 150 mM NaCl, 2 mM DTT), and PL^{pro} protein was eluted from Ni-NTA with 300 mM imidazole. Eluted PL^{pro} was dialyzed against 100-fold volume dialysis buffer (50 mM Tris [pH 7.5], 150 mM NaCl, 2 mM DTT) in a 10 000 kDa molecular weight cutoff dialysis tubing.

https://dx.doi.org/10.1021/acsptsci.0c00130
ACS Pharmacol. Transl. Sci. 2020, 3, 1265−1277

EV-A71 2A^{pro}. The EV-A71 2A^{pro} gene from strain EV-A71/7D3 (genbank accession number MF973167) with *E. coli* codon optimization was ordered from GenScript in the pET28b(+) vector. The expression and purification of EV-A71 2A^{pro} is same as that for SARS-CoV-2 PL^{pro} described in the above section.

EV-A71 3C^{pro}. The EV-A71 3C^{pro} gene from strain EV-A71/7D3 (genbank accession number MF973167) with *E. coli* codon optimization was ordered from GenScript in the pET28b(+) vector. The expression and purification of EV-A71 3C^{pro} is same as that for SARS-CoV-2 PL^{pro} described in the above section.

EV-D68 2A^{pro}. The EV-D68 2A^{pro} gene from strain US/KY/14−18953 with *E. coli* codon optimization was ordered from GenScript in the pET28b(+) vector. The expression and purification of EV-D68 2A^{pro} was described as previously.[34]

EV-D68 3C^{pro}. The EV-AD68 3C^{pro} gene from strain US/KY/14−18953 with *E. coli* codon optimization was ordered from GenScript in the pET28b(+) vector. The expression and purification of EV-D68 3C^{pro} is same as that for SARS-CoV-2 PL^{pro} described in the above section.

FRET Substrate Peptide Synthesis. The FRET-based peptide substrates used for the enzymatic assay are shown below:

- SARS-CoV-2 M^{pro} substrate: Dabcyl-KTSAVLQ/SGFRKME-Edans
- SARS-CoV-2 PL^{pro} substrate: Dabcyl-FTLRGG/APTKV-Edans
- EV-A71 2A^{pro} substrate: Dabcyl-TAITTL/GKFGQE-Edans
- EV-A71 3C^{pro} substrate: Dabcyl-IEALFQ/GPPKFRE-Edans
- EV-D68 2A^{pro} substrate: Dabcyl-KIRIVNT/GPGFGGE-Edans
- EV-D68 3C^{pro} substrate: Dabcyl-KEALFQ/GPPQFE-Edans

The synthesis of SARS-CoV-2 M^{pro}, PL^{pro}, EV-A71 2A^{pro}, EV-D68 2A^{pro} ,and EV-D68 3C^{pro} substrates were described previously.[11,34]

Enzymatic Assays. The IC_{50} values of the testing compounds against various SARS-CoV-2, EV-A71, and EV-D68 proteases in the presence or in the absence of 4 mM DTT were measured with a common protocol as the following: First, 100 μL of protease (SARS-CoV-2 M^{pro} at 100 nM; SARS-CoV-2 PL^{pro} at 200 nM; EV-A71 2A^{pro} at 3 μM; EV-A71 3C^{pro} at 2 μM; EV-D68 2A^{pro} at 1 μM; or EV-D68 3C^{pro} at 100 nM) was incubated with various concentrations of testing inhibitors at 30 °C for 30 min in its reaction buffer in a 96-well plate, and then the reaction was initiated by adding FRET substrate (SARS-CoV-2 M^{pro} and PL^{pro} substrates at 10 μM; EV-A71 and EV-D68 substrates at 20 μM). The reaction was monitored for 2 h, and the initial velocity was calculated using the data from the first 15 min by linear regression. The IC_{50} was calculated by plotting the initial velocity against various concentrations of testing inhibitor by using a four parameters dose−response curve in Prism (v8.0) software. The reaction buffers used were as follows:

- SARS-CoV-2 M^{pro} reaction buffer: 20 mM HEPES, pH 6.5, 120 mM NaCl, 0.4 mM EDTA, and 20% glycerol
- SARS-CoV-2 PL^{pro} reaction buffer: 50 mM HEPES, pH7.5, 0.01% triton X-100
- EV-A71 2A^{pro} reaction buffer: 50 mM Tris pH 7.0, 150 mM NaCl, 10% glyceol
- EV-A71 3C^{pro} reaction buffer: 50 mM Tris pH 7.0, 150 mM NaCl, 1 mM EDTA, 10% glycerol
- EV-D68 2A^{pro} reaction buffer: same as EV-A71 2A^{pro} reaction buffer
- EV-D68 3C^{pro} reaction buffer: same as EV-A71 3C^{pro} reaction buffer

Thermal Shift Binding Assay (TSA). The thermal shift binding assay (TSA) was carried out using a Thermal Fisher QuantStudio 5 Real-Time PCR System as described previously.[34,36] Briefly, 3 μM protease in its enzymatic reaction buffer (see the "Enzymatic Assays" section for the reaction buffer components) in the presence of 4 mM DTT or in the absence of DTT was incubated with testing compounds at 30 °C for 30 min in a 96-well PCR plate. SYPRO orange dye (1×) was added, and the fluorescence of the well was monitored under a temperature gradient range from 20 to 90 °C with 0.05 °C/s incremental step. The melting temperature (T_m) was calculated as the mid log of the transition phase from the native to the denatured protein using a Boltzmann model (Protein Thermal Shift Software v1.3).

Native Mass Spectrometry. The native MS binding assay of SARS-CoV-2 M^{pro} was carried out using previously described methods.[11] Briefly, purified SARS-CoV-2 M^{pro} was buffer exchanged into 0.2 M ammonium acetate (pH 6.8) at a protein concentration of 6 μM. Each of the ligands tested (GC376, ebselen, disulfiram, tideglusib, carmofur, shikonin, and PX-12) was diluted to 200 and 100 μM in ethanol. The compounds were then titrated into the protein sample to give a final drug concentration of 10, 20, or 40 μM. For the ligand binding studies containing dithiothreitol (DTT), a 40 mM stock of DTT was dissolved in water. A final concentration of 4 mM DTT was added to each of those samples. For the ligand binding studies without DTT added, an equal volume of nanopore water was added to the samples in place of DTT. The final concentration of protein in each of the samples was 4.9 μM. Each sample contained 4.5 μL of protein, 0.5 μL of ligand, and 0.5 μL of DTT or water. The samples were mixed and incubated at room temperature for 30 min prior to analysis.

Native MS was performed as previously described using Q-Exactive HF quadrupole-Orbitrap mass spectrometer with the Ultra-High Mass Range (UHMR) research modifications (Thermo Fisher Scientific). All of the samples were ionized in positive ion mode using 0.9 kV capillary voltage with the temperature set to 200 °C. The resolution of the instrument was set to 15 000 for all samples except for samples containing the compound Jun8−38−3, for which the resolution was set to 30 000. The trapping gas pressure within the instrument was set to 3.50 V of source fragmentation was applied for each of the samples to aid in desolvation of the sample. All samples were analyzed between a 500−15 000 m/z range. All of the data were deconvolved and analyzed using UniDec.[45]

Cytopathic Effect Assay (CPE). The EC_{50} and CC_{50} values for the protease inhibitors investigated in this study were measured using RD cells as described previously.[36] Briefly, RD cells were seeded and grown overnight to ∼90% confluence in a 96-well plate at 37 °C and 5% CO_2. For EV-D68 virus infection, cells were washed with PBS saline and infected with virus diluted in DMEM medium with 2% FBS and 30 mM $MgCl_2$. Viruses were incubated with cells for 1 h at

https://dx.doi.org/10.1021/acsptsci.0c00130
ACS Pharmacol. Transl. Sci. 2020, 3, 1265−1277

33 °C followed by addition of various concentrations of testing protease inhibitors in DMEM medium with 30 mM $MgCl_2$. For EV-A71 virus infection, the procedures are identical to those for EV-D68 virus, except that 30 mM $MgCl_2$ was omitted in all the media, and viruses were infected and incubated at 37 °C instead of 33 °C. Three days after infection, cells were stained with 66 μg/mL of neutral red dye for 2 h, and neutral red uptake was measured at an absorbance at 540 nM. CC_{50} was measured similarly but in the absence of viral infection.

AUTHOR INFORMATION

Corresponding Author

Jun Wang − *Department of Pharmacology and Toxicology, College of Pharmacy, The University of Arizona, Tucson, Arizona 85721, United States;* orcid.org/0000-0002-4845-4621; Phone: 520-626-1366; Email: junwang@pharmacy.arizona.edu; Fax: 520-626-0749

Authors

Chunlong Ma − *Department of Pharmacology and Toxicology, College of Pharmacy, The University of Arizona, Tucson, Arizona 85721, United States*

Yanmei Hu − *Department of Pharmacology and Toxicology, College of Pharmacy, The University of Arizona, Tucson, Arizona 85721, United States*

Julia Alma Townsend − *Department of Chemistry and Biochemistry, The University of Arizona, Tucson, Arizona 85721, United States*

Panagiotis I. Lagarias − *Department of Pharmaceutical Chemistry, Faculty of Pharmacy, National and Kapodistrian University of Athens, Athens 15771, Greece*

Michael Thomas Marty − *Department of Chemistry and Biochemistry, The University of Arizona, Tucson, Arizona 85721, United States;* orcid.org/0000-0001-8115-1772

Antonios Kolocouris − *Department of Pharmaceutical Chemistry, Faculty of Pharmacy, National and Kapodistrian University of Athens, Athens 15771, Greece;* orcid.org/0000-0001-6110-1903

Complete contact information is available at: https://pubs.acs.org/10.1021/acsptsci.0c00130

Author Contributions

C.M. performed the enzymatic and thermal shift binding assays. Y.H. performed the EV-A71 and EV-D68 antiviral assays. J.A.T. performed the native mass spectrometry binding assay under the guidance of M.T.M. P.L. performed the molecular dynamics simulations under the guidance of A.K.J.W. designed and supervised this study. C.M. and J.W. wrote the manuscript with contributions from other authors.

Notes

The authors declare no competing financial interest.

ACKNOWLEDGMENTS

This research was supported by the National Institutes of Health (NIH) (Grants AI147325 and AI157046) and the Arizona Biomedical Research Centre Young Investigator grant (ADHS18-198859) to J.W. J.A.T. and M.T.M. were funded by the National Institute of General Medical Sciences, NIH (Grant R35 GM128624 to M.T.M.). We thank Chiesi Hellas which supported this research (SARG No 10354) and the Hellenic State Scholarships Foundation (IKY) for providing a Ph.D fellowship to P.L. (MIS 5000432 and NSRF 2014-2020). This work was supported by computational time granted from the Greek Research & Technology Network (GRNET) in the National HPC facility, ARIS, under project IDs pr002021 and pr001004.

REFERENCES

(1) Zhou, P., Yang, X. L., Wang, X. G., Hu, B., Zhang, L., Zhang, W., Si, H. R., Zhu, Y., Li, B., Huang, C. L., Chen, H. D., Chen, J., Luo, Y., Guo, H., Jiang, R. D., Liu, M. Q., Chen, Y., Shen, X. R., Wang, X., Zheng, X. S., Zhao, K., Chen, Q. J., Deng, F., Liu, L. L., Yan, B., Zhan, F. X., Wang, Y. Y., Xiao, G. F., and Shi, Z. L. (2020) A pneumonia outbreak associated with a new coronavirus of probable bat origin. *Nature 579*, 270−273.

(2) Andersen, K. G., Rambaut, A., Lipkin, W. I., Holmes, E. C., and Garry, R. F. (2020) The proximal origin of SARS-CoV-2. *Nat. Med. 26*, 450−452.

(3) Funk, C. D., Laferriere, C., and Ardakani, A. (2020) A Snapshot of the Global Race for Vaccines Targeting SARS-CoV-2 and the COVID-19 Pandemic. *Front. Pharmacol. 11*, 937.

(4) Liu, C., Zhou, Q., Li, Y., Garner, L. V., Watkins, S. P., Carter, L. J., Smoot, J., Gregg, A. C., Daniels, A. D., Jervey, S., and Albaiu, D. (2020) Research and Development on Therapeutic Agents and Vaccines for COVID-19 and Related Human Coronavirus Diseases. *ACS Cent. Sci. 6*, 315−331.

(5) Shang, J., Wan, Y., Luo, C., Ye, G., Geng, Q., Auerbach, A., and Li, F. (2020) Cell entry mechanisms of SARS-CoV-2. *Proc. Natl. Acad. Sci. U. S. A. 117*, 11727−11734.

(6) Hoffmann, M., Kleine-Weber, H., Schroeder, S., Kruger, N., Herrler, T., Erichsen, S., Schiergens, T. S., Herrler, G., Wu, N. H., Nitsche, A., Muller, M. A., Drosten, C., and Pohlmann, S. (2020) SARS-CoV-2 Cell Entry Depends on ACE2 and TMPRSS2 and Is Blocked by a Clinically Proven Protease Inhibitor. *Cell 181*, 271−280.

(7) Liu, T., Luo, S., Libby, P., and Shi, G. P. (2020) Cathepsin L-selective inhibitors: A potentially promising treatment for COVID-19 patients. *Pharmacol. Ther. 213*, 107587.

(8) Sheahan, T. P., Sims, A. C., Graham, R. L., Menachery, V. D., Gralinski, L. E., Case, J. B., Leist, S. R., Pyrc, K., Feng, J. Y., Trantcheva, I., Bannister, R., Park, Y., Babusis, D., Clarke, M. O., Mackman, R. L., Spahn, J. E., Palmiotti, C. A., Siegel, D., Ray, A. S., Cihlar, T., Jordan, R., Denison, M. R., and Baric, R. S. (2017) Broad-spectrum antiviral GS-5734 inhibits both epidemic and zoonotic coronaviruses. *Sci. Transl. Med. 9*, No. eaal3653.

(9) Sheahan, T. P., Sims, A. C., Zhou, S., Graham, R. L., Pruijssers, A. J., Agostini, M. L., Leist, S. R., Schafer, A., Dinnon, K. H., 3rd, Stevens, L. J., Chappell, J. D., Lu, X., Hughes, T. M., George, A. S., Hill, C. S., Montgomery, S. A., Brown, A. J., Bluemling, G. R., Natchus, M. G., Saindane, M., Kolykhalov, A. A., Painter, G., Harcourt, J., Tamin, A., Thornburg, N. J., Swanstrom, R., Denison, M. R., and Baric, R. S. (2020) An orally bioavailable broad-spectrum antiviral inhibits SARS-CoV-2 in human airway epithelial cell cultures and multiple coronaviruses in mice. *Sci. Transl. Med. 12*, No. eabb5883.

(10) Rut, W., Groborz, K., Zhang, L., Sun, X., Zmudzinski, M., Pawlik, B., Młynarski, W., Hilgenfeld, R., and Drag, M. (March 8, 2020) Substrate specificity profiling of SARS-CoV-2 M^{pro} protease provides basis for anti-COVID-19 drug design. *bioRxiv (Biochemistry)*, 2020.2003.2007.981928, DOI: 10.1101/2020.03.07.981928.

(11) Ma, C., Sacco, M. D., Hurst, B., Townsend, J. A., Hu, Y., Szeto, T., Zhang, X., Tarbet, B., Marty, M. T., Chen, Y., and Wang, J. (2020) Boceprevir, GC-376, and calpain inhibitors II, XII inhibit SARS-CoV-2 viral replication by targeting the viral main protease. *Cell Res. 30*, 678−692.

(12) Jin, Z., Du, X., Xu, Y., Deng, Y., Liu, M., Zhao, Y., Zhang, B., Li, X., Zhang, L., Peng, C., Duan, Y., Yu, J., Wang, L., Yang, K., Liu, F., Jiang, R., Yang, X., You, T., Liu, X., Yang, X., Bai, F., Liu, H., Liu, X., Guddat, L. W., Xu, W., Xiao, G., Qin, C., Shi, Z., Jiang, H., Rao, Z., and Yang, H. (2020) Structure of M(pro) from SARS-CoV-2 and discovery of its inhibitors. *Nature 582*, 289−293.

(13) Dai, W., Zhang, B., Jiang, X. M., Su, H., Li, J., Zhao, Y., Xie, X., Jin, Z., Peng, J., Liu, F., Li, C., Li, Y., Bai, F., Wang, H., Cheng, X., Cen, X., Hu, S., Yang, X., Wang, J., Liu, X., Xiao, G., Jiang, H., Rao, Z., Zhang, L. K., Xu, Y., Yang, H., and Liu, H. (2020) Structure-based design of antiviral drug candidates targeting the SARS-CoV-2 main protease. *Science 368*, 1331−1335.

(14) Zhang, L., Lin, D., Sun, X., Curth, U., Drosten, C., Sauerhering, L., Becker, S., Rox, K., and Hilgenfeld, R. (2020) Crystal structure of SARS-CoV-2 main protease provides a basis for design of improved alpha-ketoamide inhibitors. *Science 368*, 409−412.

(15) Sacco, M. D., Ma, C., Lagarias, P., Gao, A., Townsend, J. A., Meng, X., Dube, P., Zhang, X., Hu, Y., and Kitamura, N., et al. (July 27, 2020) Structure and inhibition of the SARS-CoV-2 main protease reveals strategy for developing dual inhibitors against M^{pro} and cathepsin L. *bioRxiv (Biophysics)*, 2020.2007.2027.223727, DOI: 10.1101/2020.07.27.223727.

(16) Thenin-Houssier, S., de Vera, I. M., Pedro-Rosa, L., Brady, A., Richard, A., Konnick, B., Opp, S., Buffone, C., Fuhrmann, J., Kota, S., Billack, B., Pietka-Ottlik, M., Tellinghuisen, T., Choe, H., Spicer, T., Scampavia, L., Diaz-Griffero, F., Kojetin, D. J., and Valente, S. T. (2016) Ebselen, a Small-Molecule Capsid Inhibitor of HIV-1 Replication. *Antimicrob. Agents Chemother. 60*, 2195−2208.

(17) de Munnik, M., Lohans, C. T., Lang, P. A., Langley, G. W., Malla, T. R., Tumber, A., Schofield, C. J., and Brem, J. (2019) Targeting the Mycobacterium tuberculosis transpeptidase LdtMt2 with cysteine-reactive inhibitors including ebselen. *Chem. Commun. 55*, 10214−10217.

(18) Azad, G. K., Singh, V., Mandal, P., Singh, P., Golla, U., Baranwal, S., Chauhan, S., and Tomar, R. S. (2014) Ebselen induces reactive oxygen species (ROS)-mediated cytotoxicity in Saccharomyces cerevisiae with inhibition of glutamate dehydrogenase being a target. *FEBS Open Bio 4*, 77−89.

(19) Bender, K. O., Garland, M., Ferreyra, J. A., Hryckowian, A. J., Child, M. A., Puri, A. W., Solow-Cordero, D. E., Higginbottom, S. K., Segal, E., Banaei, N., Shen, A., Sonnenburg, J. L., and Bogyo, M. (2015) A small-molecule antivirulence agent for treating Clostridium difficile infection. *Sci. Transl. Med. 7*, No. 306ra148.

(20) Goins, C. M., Dajnowicz, S., Thanna, S., Sucheck, S. J., Parks, J. M., and Ronning, D. R. (2017) Exploring Covalent Allosteric Inhibition of Antigen 85C from Mycobacterium tuberculosis by Ebselen Derivatives. *ACS Infect. Dis. 3*, 378−387.

(21) Mukherjee, S., Weiner, W. S., Schroeder, C. E., Simpson, D. S., Hanson, A. M., Sweeney, N. L., Marvin, R. K., Ndjomou, J., Kolli, R., Isailovic, D., Schoenen, F. J., and Frick, D. N. (2014) Ebselen inhibits hepatitis C virus NS3 helicase binding to nucleic acid and prevents viral replication. *ACS Chem. Biol. 9*, 2393−2403.

(22) Nikawa, T., Schuch, G., Wagner, G., and Sies, H. (1994) Interaction of ebselen with glutathione S-transferase and papain in vitro. *Biochem. Pharmacol. 47*, 1007−1012.

(23) Leroux, F., Bosc, D., Beghyn, T., Hermant, P., Warenghem, S., Landry, V., Pottiez, V., Guillaume, V., Charton, J., Herledan, A., Urata, S., Liang, W., Sheng, L., Tang, W. J., Deprez, B., and Deprez-Poulain, R. (2019) Identification of ebselen as a potent inhibitor of insulin degrading enzyme by a drug repurposing screening. *Eur. J. Med. Chem. 179*, 557−566.

(24) Zmudzinski, M., Rut, W., Olech, K., Granda, J., Giurg, M., Burda-Grabowska, M., Zhang, L., Sun, X., Lv, Z., and Nayak, D., et al. (August 31, 2020) Ebselen derivatives are very potent dual inhibitors of SARS-CoV-2 proteases - PL^{pro} and M^{pro} in in vitro studies. *bioRxiv (Biochemistry)*, 2020.2008.2030.273979, DOI: 10.1101/2020.08.30.273979.

(25) Paranjpe, A., Zhang, R., Ali-Osman, F., Bobustuc, G. C., and Srivenugopal, K. S. (2014) Disulfiram is a direct and potent inhibitor of human O 6 -methylguanine-DNA methyltransferase (MGMT) in brain tumor cells and mouse brain and markedly increases the alkylating DNA damage. *Carcinogenesis 35*, 692−702.

(26) Diaz-Sanchez, A. G., Alvarez-Parrilla, E., Martinez-Martinez, A., Aguirre-Reyes, L., Orozpe-Olvera, J. A., Ramos-Soto, M. A., Nunez-Gastelum, J. A., Alvarado-Tenorio, B., and de la Rosa, L. A. (2016) Inhibition of Urease by Disulfiram, an FDA-Approved Thiol Reagent Used in Humans. *Molecules 21*, 1628.

(27) Galkin, A., Kulakova, L., Lim, K., Chen, C. Z., Zheng, W., Turko, I. V., and Herzberg, O. (2014) Structural basis for inactivation of Giardia lamblia carbamate kinase by disulfiram. *J. Biol. Chem. 289*, 10502−10509.

(28) Lin, M.-H., Moses, D. C., Hsieh, C.-H., Cheng, S.-C., Chen, Y.-H., Sun, C.-Y., and Chou, C.-Y. (2018) Disulfiram can inhibit MERS and SARS coronavirus papain-like proteases via different modes. *Antiviral Res. 150*, 155−163.

(29) Dementiev, A., Joachimiak, A., Nguyen, H., Gorelik, A., Illes, K., Shabani, S., Gelsomino, M., Ahn, E. E., Nagar, B., and Doan, N. (2019) Molecular Mechanism of Inhibition of Acid Ceramidase by Carmofur. *J. Med. Chem. 62*, 987−992.

(30) Huber, K., Patel, P., Zhang, L., Evans, H., Westwell, A. D., Fischer, P. M., Chan, S., and Martin, S. (2008) 2-[(1-methylpropyl)-dithio]-1H-imidazole inhibits tubulin polymerization through cysteine oxidation. *Mol. Cancer Ther. 7*, 143−151.

(31) Domínguez, J. M., Fuertes, A., Orozco, L., del Monte-Millán, M., Delgado, E., and Medina, M. (2012) Evidence for Irreversible Inhibition of Glycogen Synthase Kinase-3β by Tideglusib. *J. Biol. Chem. 287*, 893−904.

(32) Jin, Z., Zhao, Y., Sun, Y., Zhang, B., Wang, H., Wu, Y., Zhu, Y., Zhu, C., Hu, T., Du, X., Duan, Y., Yu, J., Yang, X., Yang, X., Yang, K., Liu, X., Guddat, L. W., Xiao, G., Zhang, L., Yang, H., and Rao, Z. (2020) Structural basis for the inhibition of SARS-CoV-2 main protease by antineoplastic drug carmofur. *Nat. Struct. Mol. Biol. 27*, 529−532.

(33) Ratia, K., Pegan, S., Takayama, J., Sleeman, K., Coughlin, M., Baliji, S., Chaudhuri, R., Fu, W., Prabhakar, B. S., Johnson, M. E., Baker, S. C., Ghosh, A. K., and Mesecar, A. D. (2008) A noncovalent class of papain-like protease/deubiquitinase inhibitors blocks SARS virus replication. *Proc. Natl. Acad. Sci. U. S. A. 105*, 16119−16124.

(34) Musharrafieh, R., Ma, C., Zhang, J., Hu, Y., Diesing, J. M., Marty, M. T., and Wang, J. (2019) Validating Enterovirus D68−$2A^{pro}$ as an Antiviral Drug Target and the Discovery of Telaprevir as a Potent D68−$2A^{pro}$ Inhibitor. *J. Virol. 93*, No. e02221-18.

(35) Freitas, B. T., Durie, I. A., Murray, J., Longo, J. E., Miller, H. C., Crich, D., Hogan, R. J., Tripp, R. A., and Pegan, S. D. (2020) Characterization and Noncovalent Inhibition of the Deubiquitinase and deISGylase Activity of SARS-CoV-2 Papain-Like Protease. *ACS Infect. Dis. 6*, 2099−2109.

(36) Ma, C., Hu, Y., Zhang, J., Musharrafieh, R., and Wang, J. (2019) A Novel Capsid Binding Inhibitor Displays Potent Antiviral Activity against Enterovirus D68. *ACS Infect. Dis. 5*, 1952−1962.

(37) Ma, C., Hu, Y., Zhang, J., and Wang, J. (2020) Pharmacological Characterization of the Mechanism of Action of RS23062, a Promising Antiviral for Enterovirus D68. *ACS Infect. Dis. 6*, 2260−2270.

(38) Musharrafieh, R., Kitamura, N., Hu, Y., and Wang, J. (2020) Development of broad-spectrum enterovirus antivirals based on quinoline scaffold. *Bioorg. Chem. 101*, 103981.

(39) Zhou, Q. A., Kato-Weinstein, J., Li, Y., Deng, Y., Granet, R., Garner, L., Liu, C., Polshakov, D., Gessner, C., and Watkins, S. (2020) Potential Therapeutic Agents and Associated Bioassay Data for COVID-19 and Related Human Coronavirus Infections. *ACS Pharmacol. Transl. Sci.* DOI: 10.1021/acsptsci.0c00074

(40) Pedersen, N. C., Kim, Y., Liu, H., Galasiti Kankanamalage, A. C., Eckstrand, C., Groutas, W. C., Bannasch, M., Meadows, J. M., and Chang, K. O. (2018) Efficacy of a 3C-like protease inhibitor in treating various forms of acquired feline infectious peritonitis. *J. Feline Med. Surg. 20*, 378−392.

(41) Kim, Y., Liu, H., Galasiti Kankanamalage, A. C., Weerasekara, S., Hua, D. H., Groutas, W. C., Chang, K. O., and Pedersen, N. C. (2016) Reversal of the Progression of Fatal Coronavirus Infection in Cats by a Broad-Spectrum Coronavirus Protease Inhibitor. *PLoS Pathog. 12*, No. e1005531.

(42) Sies, H., and Parnham, M. J. (2020) Potential therapeutic use of ebselen for COVID-19 and other respiratory viral infections. *Free Radical Biol. Med. 156*, 107−112.
(43) Menéndez, C. A., Byléhn, F., Perez-Lemus, G. R., Alvarado, W., and de Pablo, J. J. (2020) Molecular characterization of ebselen binding activity to SARS-CoV-2 main protease. *Sci. Adv. 6*, No. eabd0345.
(44) Tan, C. W., Tee, H. K., Lee, M. H., Sam, I. C., and Chan, Y. F. (2016) Enterovirus A71 DNA-Launched Infectious Clone as a Robust Reverse Genetic Tool. *PLoS One 11*, No. e0162771.
(45) Marty, M. T., Baldwin, A. J., Marklund, E. G., Hochberg, G. K., Benesch, J. L., and Robinson, C. V. (2015) Bayesian deconvolution of mass and ion mobility spectra: from binary interactions to polydisperse ensembles. *Anal. Chem. 87*, 4370−4376.

https://dx.doi.org/10.1021/acsptsci.0c00130
ACS Pharmacol. Transl. Sci. 2020, 3, 1265−1277